Bollettino di Geofisica Teorica ed Applicata Vol. 58, n. 1, pp. 43-54; March 2017
DOI 10.4430/bgta0185

Sensitivity analysis of marine Controlled-Source Electromagnetic data

A.H. Mansi[1], S. Marzi[2], E. Farshchiansadegh[2] and G. Bernasconi[3]

[1] *Department of Civil and Environmental Engineering, Politecnico di Milano, Italy*
[2] *Environmental and Geomatics Engineering, Politecnico di Milano, Italy*
[3] *Department of Electronics, Information, and Bio-Engineering, Politecnico di Milano, Italy*

(Received: October 18, 2016; accepted: February 27, 2017)

ABSTRACT Electromagnetic sounding methods represent one of the few geophysical techniques that can provide information about the state and the properties of deep continental crust and upper mantle. In particular, marine Controlled-Source Electromagnetic (mCSEM) method is being applied to offshore hydrocarbon exploration and providing encouraging results, as it can complement the information obtained from seismic elaborations, mainly the position of the elastic discontinuities, with a map of electrical conductivity, the principal "discriminator" between conductive water-bearing rocks and non-conductive hydrocarbon accumulations. The processing of mCSEM data can be problematic due to the non-uniqueness of the solution, the environmental and equipment noise, and the high computational power required when dealing with 3D inversion. This paper proposes a simplified procedure to study and rank the sensitivity of mCSEM in a canonical 1D scenario, with a single resistive anomaly embedded in a homogeneous background. We analyze the sensitivity of the data with respect to the most important test parameters, namely the frequency, target depth, thickness, and resistivity. In addition, this procedure is also utilized to validate the so-called T-equivalence theorem. The results of this study could assist the interpreter to highlight the reliability of the inverted parameters in a complex inversion environment.

Key words: sensitivity analysis, marine Controlled-Source Electromagnetic, mCSEM, inversion, derivatives, Residuals Versus Distance Model.

1. Introduction

Measurements of the electrical resistivity beneath the seafloor have traditionally played a crucial role in hydrocarbon exploration (Eidesmo *et al.*, 2002). Electromagnetic (EM) sounding methods represent one of the few geophysical techniques that can provide information about the current state and properties of the deep continental crust and upper mantle (Boerner, 1992).

The classical EM methods use the temporal variations of natural sources to map the conductivity of the Earth's mantle. Controlled-Source EM (CSEM) methods are an attractive complement or alternative to natural source sounding [e.g., magnetotelluric method (MT)] that is sensitive to conductive bodies (Goldstein and Strangway, 1975) and has several applications in geothermal explorations (Volpi *et al.*, 2003), in some circumstances. The position of the artificial source can be

© 2017 – OGS

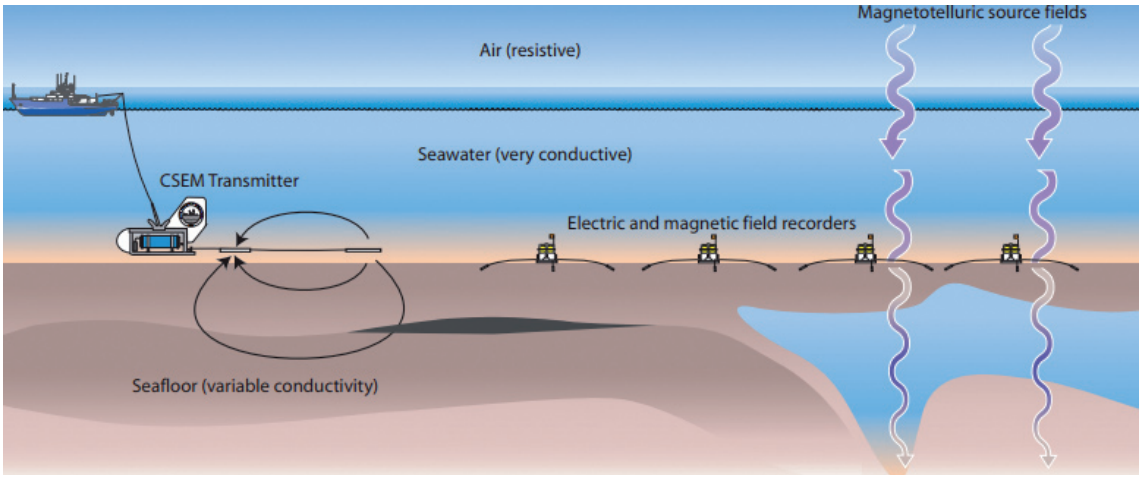

Fig. 1 - Schematic representation of the horizontal electric dipole-dipole mCSEM method, which shows an EM transmitter being towed to the seafloor to maximize the coupling of electric and magnetic fields with seafloor rocks. These fields are recorded by instruments deployed on the seafloor at some distance from the transmitter. Seafloor instruments are also able to record magnetotelluric fields that have propagated downwards through the seawater layer (Constable, 2006).

precisely determined in order to produce the excitation fields in an optimal geometrical form, and also the source frequency spectrum can be tailored for a particular experiment (Boerner, 1992). Marine CSEM (mCSEM) methods map the electrical resistivity of the sub-seafloor structures with a maximum resolution of a few tens of metres and a depth of investigation of several kilometres below the seafloor (Fig. 1). mCSEM methods generally use a horizontal electric dipole source towed near the seabed and an array of receiver dipoles tied to the seabed. The transmitter dipole emits a low frequency EM signal that propagates into the seawater column and downwards into the subsurface (Constable, 2006).

Diffusion of the EM field (for a particular frequency) depends on the thickness and the background resistivity of the subsurface and on the properties of the seawater column. In a high resistivity layer (e.g., caused by hydrocarbon saturation), the EM field propagates with a lower attenuation than in the less resistive surrounding sediments. This is the basic concept for the interpretation of mCSEM data: the electric field magnitude and phase versus source-receiver offset will show different trends as a function of the subsurface resistivity distribution (Dell'Aversana, 2007).

A quick way to represent mCSEM responses is to plot the amplitude and phase of the electric and magnetic fields versus a range of offsets of particular interest. One of the advantages of mCSEM surveys is that the data can be acquired either by performing a simplified 1D model or complex 3D ones (Peace *et al.*, 2004). Similarly, mCSEM data can be interpreted with simple methods, such as interpreting the results of the symmetry attribute analysis of the amplitude component (Dell'Aversana and Zanoletti, 2008, 2010) or the phase component (Ezieke *et al.*, 2016), or with complex approaches such as inversion (Dell'Aversana, 2007). In the case of mCSEM data inversion, the procedure usually needs the evaluation of a Jacobian matrix, which represents the sensitivity of the data to the model parameters. Complex mathematical approaches, such as adjoint Green's function, were used to produce numerical values for the sensitivity matrix (Farquharson, 1995).

In this paper, we present a simplified approach for evaluating the sensitivity of mCSEM with respect to the most important physical parameters, without following any complex analytical and/or numerical procedures. We consider a 1D canonical scenario, with a single resistive layer embedded in a homogeneous background below the sea bottom. The study parameters, or test parameters, are the frequency, the target depth, thickness, and resistivity. The proposed procedure consists of the following steps:

- compute numerically the Jacobian matrix of the derivatives of the data with respect to the test parameters;
- use an unconventional visual approach in the data residuals versus distance model space, in order to rank the sensitivity of the tested model parameters and their correlation.

In addition, we use the computed EM field responses to validate the so-called T-equivalence theorem (Constable, 2010), and we propose a simplified inversion procedure based on a pattern-matching step between the observed data and a set of precomputed responses.

The Jacobian matrix could be further exploited for a conditioning analysis of the inverse problem, as in Dell'Aversana *et al*. (2011), but this is out of the main scope of this paper.

2. Methodology

CSEM data inversion is generally an ill-posed problem that can be faced only by an accurate selection of the initial model and an appropriate identification of the observable parameters. The latter is a crucial task in many geophysical applications, especially when working with large models, which are thought to summarize the current scientific knowledge in a mathematical language. In this case, in order to find physically reasonable parameter values, the main tool is a sensitivity analysis (Brun *et al*., 2001).

Generally speaking, sensitivity analysis (SA) attempts to assess the variations of a model output in concordance with small variations of the model inputs given by variables or parameters (Fassò and Perri, 2002). Global SA methods offer a comprehensive analysis by evaluating the sensitivity of a certain parameter while dynamically varying the other parameters. Hence, they do not depend on the choice of any reference model (Saltelli *et al*., 2008).

Nevertheless, in order to avoid complex procedures and time-consuming calculations, we present a local SA: instead of varying the whole set of parameters in the parameters' space, the local SA approach considers the derivatives of the model output with respect to an arbitrary reference scenario (reference model). This approach has been proven to be particularly successful in cases where systems are operated around predefined parameter ranges. In addition, it is a very promising approach in cases where values of some test parameters are known *a priori*, thus increasing the reliability of the final solution and reducing the required computational resources (Brun *et al*., 2001). Also, note that the linearization of the inversion procedure gives access to the Jacobian matrix of sensitivity values, i.e., the partial derivatives of the data with respect to each test parameter (Farquharson, 1995). In the data space, we consider only the magnitude of the horizontal electric field (E_x) response. It is possible to extend the study to the other electrical and magnetic components, but, according to Key (2009), an inline horizontal electric dipole would provide better resolution than either broadside or vertical electric dipoles, and the horizontal electric and magnetic fields for any transmitter orientation have better resolution than vertical fields.

On the other hand, the magnitude of the vertical electric field response (E_z) which is not considered here, is useful for the discrimination of deep resistive targets even at very close source-receiver offsets (Alumbaugh *et al.*, 2010). Also, as a result of the work of Constable and Weiss (2006), which demonstrated that a simple 1D modelling can predict the CSEM response to a very high accuracy when compared to a complex 3D modelling, the data utilized for this research have been extracted from the 1D model proposed by Constable and Srnka (2007). This canonical model presents the amplitude and phase curves versus source-receiver offset of a 100-m thick oilfield reservoir, 100 Ω·m, buried at a depth of 1000 m, in a host sediment layer of 1 Ω·m under a 1000 m seawater column. Water conductivity is σ=4 S/m. The values reported here are the reference scenario. Using the reference scenario, we define some test parameters that will vary in the simulation step. They are the frequency, the target depth, thickness, and conductivity. The ranges of the varying test parameters are reported in Table 1.

Table 1 - The reference scenario and the ranges of the test parameters.

Parameters Unit	Frequency (*f*) [Hz]	Depth (*d*) [m]	Thickness (*t*) [m]	Conductivity (σ) [S/m]
Range	0.125 – 0.75	100 – 500	10 – 500	0.01 – 1.00
Reference Model	0.5	500	100	0.20

The output responses of the model are computed for 25 receivers (R_x) tied at 1 m above the seabed and an EM field transmitting-source (T_x) towed at 20 m above the sea bottom. The maximum considered offset (distance between transmitter and receiver) is 10000 m. Fig. 2 summarizes all the different layers and their fixed and varying test parameters.

The proprietary simulator, based on the Sommerfeld integral, needs a 1D model defined by layers and their resistivity, and computes the magnitude versus offset (MVO) and phase versus offset (PVO) of the inline electrical component.

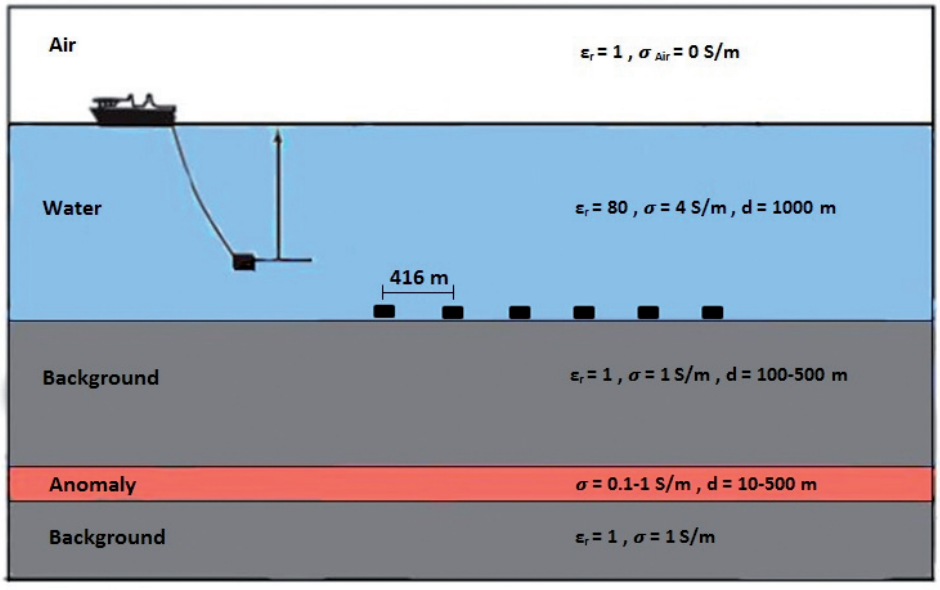

Fig. 2 - Model description.

2.1. Derivative approach

We compute the derivatives with the central finite difference approximation, reported in Eq. 1 (Luz *et al.*, 2013):

$$\frac{\partial (E_x)}{\partial p} \approx \frac{E_{x p_{ref}+\Delta_p} - E_{x p_{ref}-\Delta_p}}{2\Delta_p} \tag{1}$$

where p is a generic test parameter, p_{ref} is the value of p in the reference scenario, Δ_p is the infinitesimal increment of p, and E_x is the electric field component in the x directions at each receiver.

In order to perform the SA, all the derivatives should be mutually compared. Hence, all the computed derivatives should contain identical dimensions or be dimensionless. Consequently, the solution to such a challenge is either to normalize all the scales and/or cancel all the dimensions. First, the various parameters' ranges are rescaled into a fixed 0,1 range utilizing the min-max scale normalization of Eq. 2:

$$p^n = \frac{p - p_{min}}{p_{max} - p_{min}} \tag{2}$$

Instead to cancel the dimensions, the suggested solution is to divide the evaluated derivatives by the magnitude of the derivatives of the reference scenario (as reported in Eq. 3):

$$\frac{d (E_x)}{dp} = \frac{\frac{\partial (E_x)}{\partial p}}{\frac{E_{x p_{ref}}}{\Delta_p}} = \frac{\frac{E_{x p_{ref}+\Delta_p} - E_{x p_{ref}-\Delta_p}}{2\Delta_p}}{\frac{E_{x p_{ref}}}{\Delta_p}} \tag{3}$$

where p is a generic test parameter, Δ_p is the infinitesimal increment of p, and p_{min}, p_{max}, and p^n are the minimum, maximum, and normalized value of the parameter p, respectively.

In this formulation we have used an increment of 0.1% for all the parameters, one at a time, to numerically compute the variation of the data. Moreover, in order to draw general conclusions, several reference models should be tested. We have computed the derivatives for values of the reference scenario in the extremes of a realistic range of values: this analysis (not reported within this manuscript) shows similar trends of the derivatives.

2.2. Visual approach

This section will thoroughly illustrate the steps followed in order to build the residuals versus distance model that permits the visual inspection of the sensitivity and of the structure of the inversion problem. In fact, the inversion aims at minimizing an objective function, generally the residual sum of squares (RSS) between observed data and the same data computed in a trial model (Dell'Aversana *et al.*, 2011). In our mCSEM study, the residual axis reports an RSS between the magnitude of the electrical field E_{x_i} computed for a set i of test parameters and the magnitude of the electrical field for the reference test parameters, $E_{x_{ref}}$, as reported in Eq. 4:

$$RSS = \sum_{n=1}^{n} \left(|E_{x_i}| - |E_{x ref}| \right)^2. \tag{4}$$

The other axis is the Euclidean distance between the trial set of parameters and the reference one (Eq. 5), as presented in Bosisio *et al.* (2014). Although we are studying the sensitivity with

respect to the frequency, which is in reality a known parameter, and it does not belong to the model space of parameters, hereafter we call model *i* the *i-th* set of test parameters (so comprising the frequency and, if described, any other variable parameter):

$$d_{i,ref} = \sqrt{\left(f_i^n - f_{ref}^n\right)^2 + \left(\sigma_i^n - \sigma_{ref}^n\right)^2 + \left(t_i^n - t_{ref}^n\right)^2 + \left(d_i^n - d_{ref}^n\right)^2}. \quad (5)$$

As in Eq. 5, $d_{i,ref}$ is the distance between the *i-th* model and the chosen reference model; f_i^n, σ_i^n, t_i^n, and d_i^n are the normalized frequency, conductivity, thickness, and depth of the *i-th* model, respectively, f_{ref}^n, σ_{ref}^n, t_{ref}^n, and d_{ref}^n are the normalized frequency, conductivity, thickness, and depth of the reference model, respectively; n stands for the number of horizontally placed receivers on the seafloor (i.e., 25 for our study); and E_{xi} and E_{xref} represent the magnitude of the computed electrical field of the *i-th* and the reference model, respectively.

The analysis is performed by selecting the trial models, i.e., by defining a discretization of the test parameters within their range of variation. We use 1000 intervals per parameter, with an incremental spacing, Δ, equivalent to 0.1% of the whole normalized variation interval. The trial model data set is built as shown in the matrix (Eq. 6), explained as follows:

- a single test parameter of the reference model varies over the full normalized range while keeping the other three test parameters undisturbed;
- a single test parameter of the reference model varies over the full normalized range, while perturbing the other parameters, one at a time with increments of $\pm m\Delta$, with m = 1, 2, 4, 8:

$$\mathbf{V_p} = \begin{bmatrix} \mathbf{f} & \sigma_{\mathbf{ref}} & \mathbf{t_{ref}} & \mathbf{d_{ref}} \\ \mathbf{f} & \sigma_{\mathbf{ref}} \pm m\Delta & \mathbf{t_{ref}} & \mathbf{d_{ref}} \\ \mathbf{f} & \sigma_{\mathbf{ref}} & \mathbf{t_{ref}} \pm m\Delta & \mathbf{d_{ref}} \\ \mathbf{f} & \sigma_{\mathbf{ref}} & \mathbf{t_{ref}} & \mathbf{d_{ref}} \pm m\Delta \\ \mathbf{f_{ref}} & \sigma & \mathbf{t_{ref}} & \mathbf{d_{ref}} \\ \mathbf{f_{ref}} \pm m\Delta & \sigma & \mathbf{t_{ref}} & \mathbf{d_{ref}} \\ \mathbf{f_{ref}} & \sigma & \mathbf{t_{ref}} \pm m\Delta & \mathbf{d_{ref}} \\ \mathbf{f_{ref}} & \sigma & \mathbf{t_{ref}} & \mathbf{d_{ref}} \pm m\Delta \\ \mathbf{f_{ref}} & \sigma_{\mathbf{ref}} & \mathbf{t} & \mathbf{d_{ref}} \\ \mathbf{f_{ref}} \pm m\Delta & \sigma_{\mathbf{ref}} & \mathbf{t} & \mathbf{d_{ref}} \\ \mathbf{f_{ref}} & \sigma_{\mathbf{ref}} \pm m\Delta & \mathbf{t} & \mathbf{d_{ref}} \\ \mathbf{f_{ref}} & \sigma_{\mathbf{ref}} & \mathbf{t} & \mathbf{d_{ref}} \pm m\Delta \\ \mathbf{f_{ref}} & \sigma_{\mathbf{ref}} & \mathbf{t_{ref}} & \mathbf{d} \\ \mathbf{f_{ref}} \pm m\Delta & \sigma_{\mathbf{ref}} & \mathbf{t_{ref}} & \mathbf{d} \\ \mathbf{f_{ref}} & \sigma_{\mathbf{ref}} \pm m\Delta & \mathbf{t_{ref}} & \mathbf{d} \\ \mathbf{f_{ref}} & \sigma_{\mathbf{ref}} & \mathbf{t_{ref}} \pm m\Delta & \mathbf{d} \end{bmatrix} \quad (6)$$

The matrix $\mathbf{V_p}$ contains all the 100075 combinations of the test parameters for perturbations $m\Delta$, with m = 1, 2, 4, and 8 and Δ = 0.1%: **f** are the 1001 normalized frequency values, σ are the 1001 normalized conductivity values, **t** are the 1001 normalized thickness values, **d** are the 1000 normalized depth values, and $\mathbf{f_{ref}}$, $\boldsymbol{\sigma}_{\mathbf{ref}}$, $\mathbf{t_{ref}}$, and $\mathbf{d_{ref}}$ stand for the reference scenario values.

The ultimate goal of this experiment is to rank the sensitivity of the investigated test parameters by inspecting how the residuals change while each test parameter varies over the full range and, also, how much a small perturbation of one test parameter impacts the RSS model-distance curve of another parameter. As an example, we will observe that a perturbation of the conductivity has a low impact in the curves obtained for variations of frequency. This can be explained in two ways:

- the model is highly sensitive to the frequency;
- the frequency is not correlated to conductivity and could be considered unbiased.

The results of this analysis are presented in a following section.

3. Validation of T-equivalence theorem

We report here a validation of the T-equivalence theorem using the data generated while populating the residuals versus distance domain. According to the T-equivalence theorem (Parasnis, 1979), the layers with identical ($\tau * \rho \equiv \frac{\tau}{\sigma}$) are electrically equivalent, where τ, ρ, and σ stand for the layer thickness, resistivity factor, and conductivity factor, respectively. For such validation, two different scenarios were considered for the selection of models with identical $\tau * \rho$ value, as shown in Fig. 3.

Scenario A alters only the thickness of the resistive layer, keeping the depth of the top surface fixed, while in Scenario B, both the thickness and the depth of the resistive layer are changed, keeping the centre of the layer fixed.

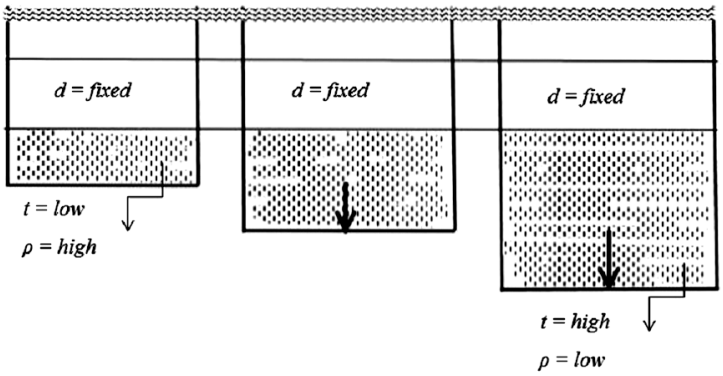

Scenario A: the top surface of the resistive layer is kept constant and the bottom surface changes (i.e., only the layer thickness changes).

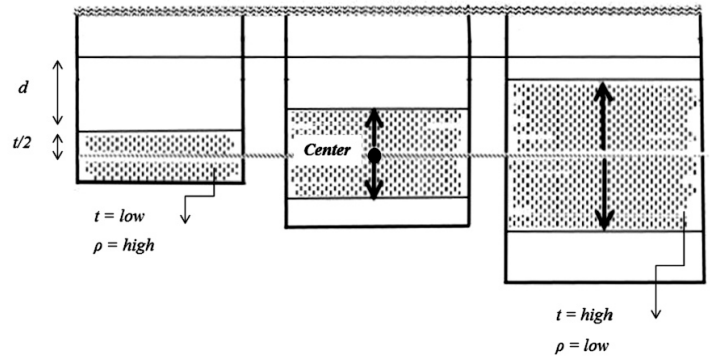

Scenario B: the centre of the resistive layer is kept constant by changing the top and the bottom surfaces (i.e., simultaneously changing the thickness and the depth of the resistive layer).

Fig. 3 - The two scenarios used for the validation.

For each scenario, a total number of 35 electrically equivalent models were extracted from the precomputed database in order to draw the residuals versus distance plots. In concordance with the hypothesis of the T-equivalence theorem, all models have $\tau*\rho = \tau_{ref}*\rho_{ref}$ = constant, where the thickness and the resistivity factor varied according to Table 1. The validation results are presented in the following sections.

4. Results and discussion

This section presents the results of the SA obtained by evaluating the Jacobian matrix and by exploring the residual-distance domain. Moreover, it shows the numerical validation of the T-equivalence theorem.

4.1. Results of the Jacobian analysis

In order to investigate which parameters are more effective and influential on the electrical response (E_x), the different partial derivatives of the electrical field magnitude with respect to the investigated test parameters (i.e., $\frac{\partial(E_x)}{\partial f}$, $\frac{\partial(E_x)}{\partial \sigma}$, $\frac{\partial(E_x)}{\partial t}$, and $\frac{\partial(E_x)}{\partial d}$) have been computed and normalized (see Fig. 4).

Frequency is the first driving parameter, especially in the middle to far offsets. Layer thickness and depth are the second ones. Interestingly, their sensitivities are complementary along the offset, suggesting that short to middle offsets could be used for the determination of the layer depth, and middle to far offsets for inferring the layer thickness. The less sensitive parameter is the layer conductivity, with a bell-shaped curve centred in the middle offset range.

From the previous discussion, we can infer that the model is highly sensitive to frequency, moderately sensitive to depth and thickness, and less sensitive to conductivity. The mCSEM model sensitivity rankings have been summarized in Table 2, while the definitive sensitivity ranking will be fulfilled in the following section.

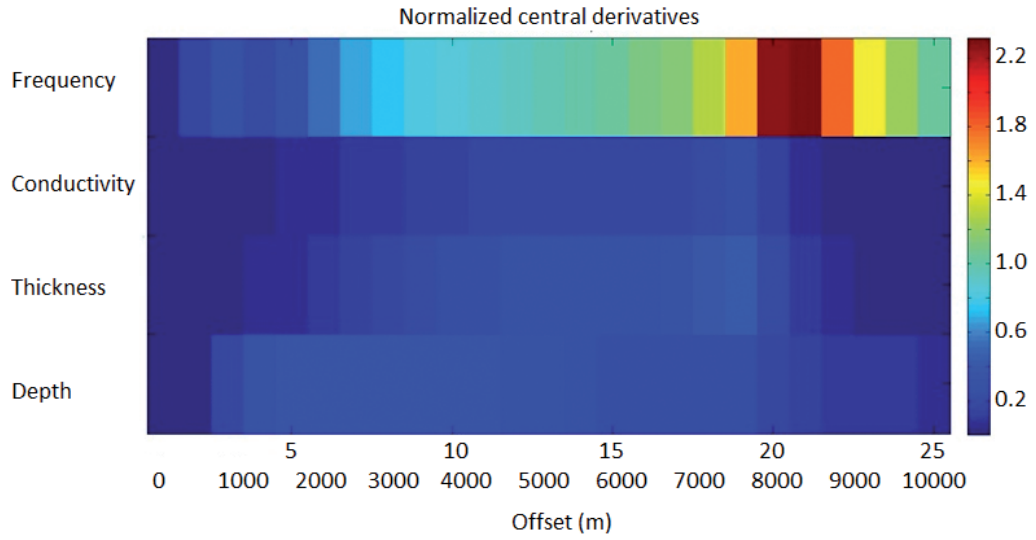

Fig. 4 - The normalized partial derivatives with respect to the test parameters.

Table 2 - The ranking and the range of the sensitivity values with respect to the test parameters.

Parameters	Frequency (f) [Hz]	Depth (d) [m]	Thickness (t) [m]	Conductivity (σ) [S/m]
Range [Descriptive]	Intensively	Moderately	Slightly	Slightly
Offset [Range]	Full Range	Short-to-relatively far	Middle	Middle
Offset [m]	Full Range	800-8400	2800-8000	4800-8000
Peak [m]	7900-8750	1700-5500	7000-7500	7000-7500

4.2. Results of the visual analysis

The electrical responses (E_x) of 100075 models described by the parameters in the matrix (see Eq. 6) have been exploited to produce the residuals versus distance plots. Some preliminary concepts are introduced to facilitate the analysis step.

First, the residuals slope could be steep and spiky or smooth and gentle. The steep and spiky curves would indicate higher variation rates with respect to variations of the reference scenario, which correspond to a high sensitivity. Second, the dispersion along the distance axis represents the correlation between the different parameters.

Fig. 5 shows the whole data set. Colors are associated with the different test parameters. Points connected to frequency variations have the highest slope, the spikiest convergence versus the global minimum, and a very small dispersion along the distance axis, meaning that sensitivity to frequency is higher than that of all other parameters. Fig. 6 shows the RSS model-distance plots separated for each parameter, plus the curve with a variation of the other parameters. When the 2Δ variation curve of a particular parameter produces a shift along the distance axis with respect to the reference model coordinate, we can conclude that the two parameters are correlated, as one influences the convergence of the other to a solution different from the true one (i.e., the reference model).

Except for frequency, all the other parameters exhibit a similar behaviour with comparable sensitivity levels, slightly higher for the layer depth. Moreover, in contrast to frequency, the trends of the other parameters (Figs. 6b, 6c, and 6d) illustrate noticeable shifts (e.g., eccentricity distance) that create local minimas, which indicate that more iterations would be required to

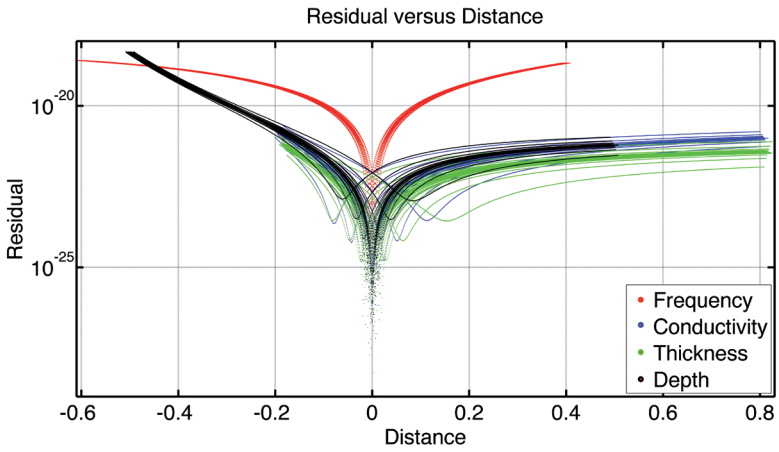

Fig. 5 - The residuals versus distance plots.

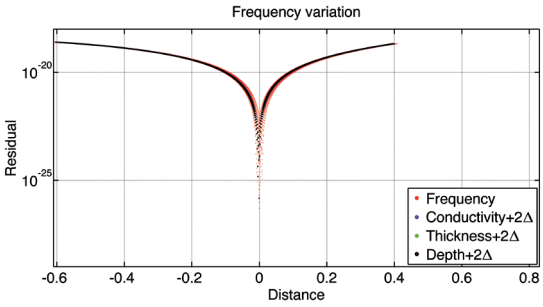

(a) Frequency residuals versus distance.

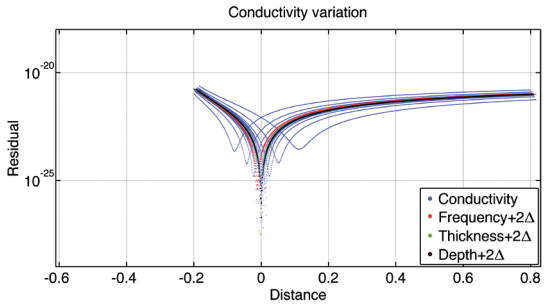

(b) Conductivity residuals versus distance.

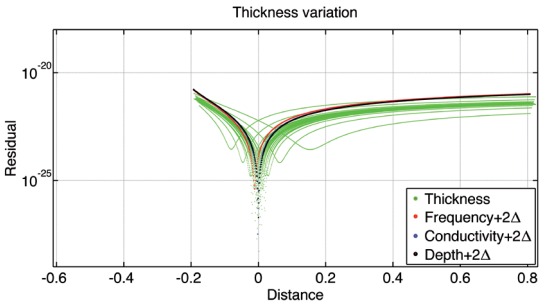

(c) Thickness residuals versus distance.

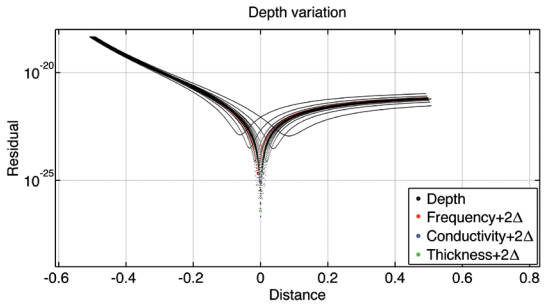

(d) Depth residuals versus distance.

Fig. 6 - The residuals versus distance.

converge towards the global minima in a complex inversion environment. Consequently, this raises an alert about the stability of any inversion procedure that might get trapped in such local minimas, whose existence can be justified by the existing correlations between the studied test parameters.

4.3. Results of the visual analysis

The residuals versus distance plots for both scenarios are shown in (Fig. 7). The T-equivalence theorem would have been definitively validated if the residuals had approximately the same value, in other words, if the residuals depicted a negligible variation. Regarding Scenario A (Fig. 7a) and Scenario B (Fig. 7b), the variation of the residuals is less than one order of magnitude. Consequently, it could be inferred that the residuals have approximately the same value and therefore the T-equivalence theorem is proven and validated. The comparison shows that the variation range of the residuals of Scenario A (Fig. 7a) is higher than the variation range of the residuals of Scenario B (Fig. 7b). Therefore, it can be interpreted that the T-equivalence assumption is more valid when the centre of the resistive layer is kept fixed.

5. Conclusion

We have presented a SA for a mCSEM 1D canonical scenario, with a single resistivity layer embedded in a homogeneous less resistive background. We have selected the frequency and the

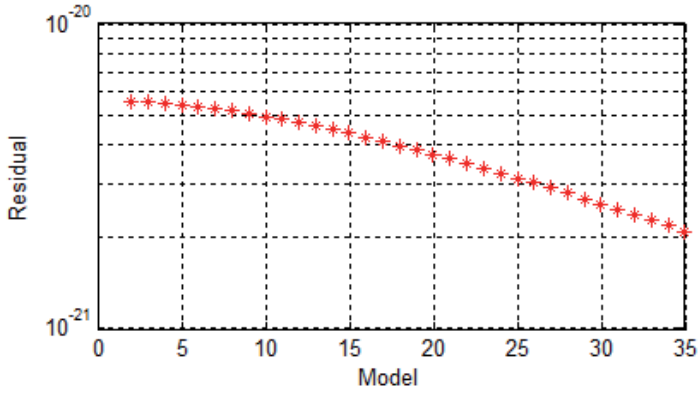

Scenario A.

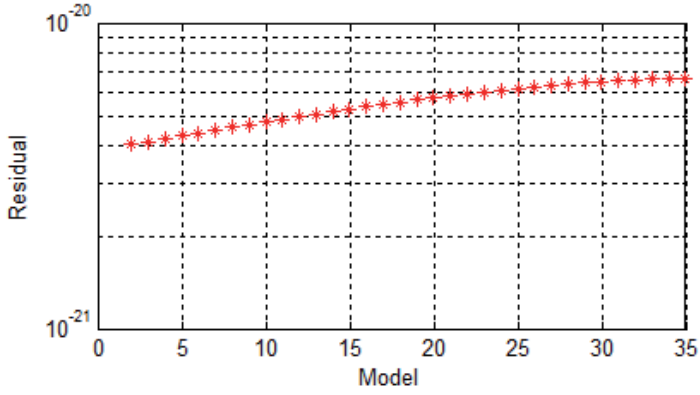

Scenario B.

Fig. 7 - Residual versus models for the validation of the T-equivalence theorem. The x-axis represents the ID associated with each of the selected 35 models and the y-axis represents residuals between the 35 selected models and the reference model.

resistive layer descriptors (thickness, depth, conductivity) as variable parameters for the evaluation of the Jacobian matrix. The results show that frequency is the predominant driver, followed by the layer geometrical parameters (depth and thickness), and finally by the layer conductivity. The inspection of the sensitivity versus offset suggests that different complementary offset ranges can be used to invert the different parameters, probably increasing the inversion efficacy and reliability. This aspect could be further investigated by analyzing the eigenvector/eigenvalues structure of the Jacobian: this topic has been addressed by some of the authors of this paper in other referenced publications.

We have also proposed a simple visual approach in order to analyze the model-data inner connection. It works in the residual model-distance domain, and it consists of evaluating the data for many models and in building the corresponding output data residuals and the input parameters distance from a reference model. The visual analysis of the cloud of points can reveal interesting properties of the inverse problem structure as well as of the correlation between the various test parameters.

Finally, we have exploited the computed models to check and validate the T-equivalence theorem, finding that it holds especially well when changing the layer thickness inversely to the resistivity factor, but keeping the depth of the centre of the layer fixed.

REFERENCES

Alumbaugh D., Cuevas N.H., Chen J., Gao G. and Brady J.; 2010: *Comparison of sensitivity and resolution with two marine CSEM exploration methods*. In: SEG Annual Meeting.

Boerner D.E.; 1992: *Controlled-source electromagnetic deep sounding: theory, results and correlation with natural source results*. Surveys in Geophysics, **13**, 435-488.

Bosisio A.V., Drufuca G. and Rovetta D.; 2014: *The concept of distance in global optimization applied to non-linear inverse problems*. Inverse Problems in Science and Engineering, **22**, 683-706.

Brun R.P., Reichert P. and Kunsch H.R.; 2001: *Practical identifiability analysis of large environmental simulation models*. Water Resources Research, **37**, 1015-1030.

Constable S.; 2006: *Marine electromagnetic methods - A new tool for offshore exploration*. The Leading Edge, **25**, 438-444.

Constable S.; 2010: *Ten years of marine CSEM for hydrocarbon exploration*. Geophysics, **75**, A67-A81.

Constable S. and Srnka L.; 2007: *An introduction to marine controlled-source electromagnetic methods for hydrocarbon exploration*. Geophysics, **72** (2), WA3-WA12.

Constable S. and Weiss C.J.; 2006: *Mapping thin resistors and hydrocarbons with marine EM methods: Insights from 1D modeling*. Geophysics, **71** (2), G43-G51.

Dell'Aversana P.; 2007: *Marine CSEM data interpretation: pitfalls and possible solutions*. The Leading Edge, **26**, 686-691.

Dell'Aversana P. and Zanoletti F.; 2008: *Accurate detection of reservoir boundaries using electromagnetic attributes and inversion of marine CSEM data*. In: The 70th EAGE Conference & Exhibition.

Dell'Aversana P. and Zanoletti F.; 2010: *Spectral analysis of marine CSEM data symmetry*. In: EGM International Workshop.

Dell'Aversana P., Bernasconi G., Miotti F. and Rovetta D.; 2011: *Joint inversion of rock properties from sonic, resistivity and density well-log measurements*. Geophysical Prospecting, **59**, 1144–1154.

Eidesmo T., Ellingsrud S., MacGregor L.M., Constable S., Sinha M.C., Johansen S.E. *et al.*; 2002: *Sea bed logging (SBL), a new method for remote and direct identification of hydrocarbon filled layers in deepwater areas*. First break, **20**, 144-152.

Ezieke A.H., Mansi A.H. and Bernasconi G.; 2016: *Investigation of symmetry attribute analysis on the phase measurements of marine controlled-source electromagnetic surveys*. Boll. Geof. Teor. Appl., **57**, 287-300.

Farquharson C.G.; 1995: *Approximate sensitivities for the multi-dimensional electromagnetic inverse problems*. Ph.D dissertation, University of British Columbia, 120 pp.

Fassò A. and Perri P.F.; 2002: *Sensitivity analysis*. In: El-Shaarawi A.H. and Piegorsch W.W. (eds), Encyclopedia of Environmetrics, Wiley, Vol. 4, pp. 1968-1982.

Goldstein M.A. and Strangway D.W.; 1975: *Audio-frequency magnetotellurics with a grounded electric dipole source*. Geophysics, **40**, 669-683.

Key K.; 2009: *1D inversion of multicomponent, multifrequency marine CSEM data: Methodology and synthetic studies for resolving thin resistive layers*. Geophysics, **74** (2), F9-F20.

Luz E.D., Silva V.D. and Régis C.; 2013: *Fast sensitivities for 2D marine CSEM inversion*. In: SEG Annual Meeting.

Parasnis D.S.; 1979: *Principles of Applied Geophysics* (Fourth ed.). Chapman and Hall, London.

Peace D., Meaux D., Johnson M. and Taylor A.; 2004: *Controlled-source electromagnetics for hydrocarbon exploration*. Houston Geological Society Bulletin, **47**, 31-45.

Saltelli A., Ratto M., Andres T., Campolongo F., Cariboni J., Gatelli D. *et al.*; 2008: *Global sensitivity analysis: the primer*. John Wiley and Sons, 292 pp.

Volpi G., Manzella A. and Fiordelisi A.; 2003: *Investigation of geothermal structures by magnetotellurics (MT): an example from the Mt. Amiata area, Italy*. Geothermics, **32**, 131-145.

Corresponding author: Ahmed H. Mansi
Department of Civil and Environmental Engineering, Politecnico di Milano
Piazza Leonardo da Vinci 32, 20133 Milano, Italy
Phone: +39 02 2399 6505; fax: +39 02 2399 2206; email: ahmed.hamdi@polimi.it